Self-consistent resonance absorption with two-layer profile steepening

E. Ahedo and J. R. Sanmartín
E.T.S.I. Aeronáuticos, Universidad Politécnica de Madrid, 28040-Madrid, Spain

(Received 8 May 1989; accepted 10 August 1989)

Resonance absorption of p-polarized light, incident at angle θ on a flowing, stratified plasma, is analyzed; profile steepening within (i) a layer around the turning point, and (ii) a thinner, embedded sublayer at the critical surface is taken into account self-consistently. The entire steepened region is taken as collisionless and isothermal. The structure of the main layer shows a variety of regimes, depending on how the flow crosses a sonic point. The structure of the sublayer is also determined; it is *entirely subsonic* (with no wave breaking) for a well-defined, broad parameter range. Density changes across both layer and sublayer, and fractional absorption, are given in terms of [(wavelength)$^2\times$intensity/temperature], θ, and (temperature/$m_e c^2$). The flow outside the double structure is also analyzed for particular conditions.

I. INTRODUCTION

In laser fusion there is a range of conditions for which inverse bremsstrahlung absorption may not be efficient enough, a non-negligible fraction of the incoming intensity reaching the reflection surface, and yet there may not be such anomalous effects as harmonic generation, hot electron populations, and so on. We consider, in particular, intensity I, wavelength λ, and electron temperature T such that $I\lambda^2/T\sim 10^{14}$–10^{15} (W/cm^2)μm^2/keV.

The reflection of the light can give rise to important coupled effects. First, the light pressure (which includes the usual time average of momentum flux due to the electron quivering velocity) locally steepens the stratified plasma profile around the turning point.[1] Additionally, the light ripples the flow downstream of that point.[2]

Second, with the electric field of the wave partly along the density gradient ∇n, i.e., for p polarization, the light tunnels through to the critical density $n_c(\lambda)$, where it excites plasma waves.[3] These waves travel down the density gradient and are eventually absorbed via Landau damping.[4] Note that this resonance absorption is quite sensitive to the scale of ∇n, and that the longitudinal field of the plasma waves produces further, highly localized, steepening.[5]

For s polarization or normal incidence, for which there is no resonance absorption, profile steepening has been carefully analyzed in the past: There is a thin reflection layer where the field goes from oscillatory to evanescent and the flow accelerates through a sonic point.[2,6,7] For p polarization, however, only incomplete analyses have been carried out. The capacitor model[5,8] was used to study just steepening and absorption around the critical surface; since the reflection phenomenon was ignored no connection to the large region of coronal plasma outside the steepened zone was possible so that no self-consistent absorption could be determined. Further, the fluid dynamics of the problem was simplified in excess. The relation between the dielectric function and wave pressure was either a static one (with an arbitrary density scale length),[9,10] or was determined by requiring the flow to become sonic in the resonance region (which we prove to be false, in general) with some *ad hoc* Landau damping[11] or an estimated scale length.[12] Absorption via collisions instead of Landau damping has also been considered[5,13] and found to be effective for weak profile steps only.

Here we perform a self-consistent, asymptotic analysis of resonance absorption and the double structure of the steepened profile for p polarization. As with s-polarized light, there is a thin quasisteady reflection layer centered at the turning point; there is also, however, a thinner, imbedded sublayer where the plasma waves are excited. The steepening makes the entire region short enough that the plasma may be assumed isothermal, and collisions neglected. A fluid model is used; a broad, well defined parameter range for which there is no wavebreaking[14] is considered. The analysis yields the dimensionless, fractional absorption in terms of λ, and values of T, I, and incidence angle θ, at the exhaust of the reflection layer, so that the results could be implemented in codes.

The basic equations, including a Bernoulli equation, are presented in Sec. II and are discussed in the Appendix. The reflection layer is analyzed in Sec. III, with the sublayer as a discontinuity. Determining its structure is reduced to a quadrature but requires a careful discussion of sonic conditions, several different regimes being proved to exist. The structure of the sublayer, studied in Sec. IV, yields the absorbed flux, with no need for a particular model of Landau damping; a broad parameter region is considered for which the entire sublayer *is subsonic*. The fractional absorption is obtained in Sec. V; for particular conditions an approximate, self-similar solution for the large coronal region outside the reflection layer is obtained. A discussion of results is given in Sec. VI.

II. BASIC EQUATIONS

We consider a stratified plasma, flowing along the negative z axis, and light of frequency ω incident from vacuum on the left at an angle θ in the y-z plane.

For p polarization, the electromagnetic wave takes the form

$$\overline{E}=E_y\overline{1}_y+E_z\overline{1}_z,\quad \overline{B}=B\overline{1}_x, \tag{1}$$

 0899-8221/89/122450-12$01.90

where all components are supposed to vary as $\exp(-i\omega t + i\omega c^{-1} y \sin\theta)$, the real part of (1) giving the field. We split the electronic variables into high- and low-frequency parts

$$n_e = n + n_{eh}, \quad \bar{v}_e = \bar{v}_{el} + \bar{v}_{eh},$$

and assume that the fast current density can be written as

$$\bar{J}_h \cong -en\bar{v}_{eh},$$

neglecting harmonic generation and wavebreaking; we discuss this approximation in the Appendix. Maxwell's equations then become

$$\frac{\partial E_y}{\partial z} = i\omega c^{-1}(E_z \sin\theta - B), \tag{2}$$

$$\frac{\partial B}{\partial z} = -i\omega c^{-1}\epsilon E_y, \tag{3}$$

$$3\lambda_D^2 \frac{\partial^2 E_z}{\partial z^2} + \epsilon E_z = B\sin\theta + E_L. \tag{4}$$

The first term in (4) is the usual dispersive effect, coming from the pressure in the linearized, high-frequency momentum equation for electrons; E_L is some phenomenological representation of (kinetic) Landau damping; $\epsilon \equiv 1 - n/n_c$ is the cold, collisionless dielectric function, to be used instead of n where convenient; and λ_D is the Debye length at the critical density $n_c(\omega)$.

The low-frequency, quasineutral, isothermal behavior is given by the ion continuity and total momentum equations

$$\frac{\partial n}{\partial t} + \frac{\partial}{\partial z} nv = 0, \tag{5}$$

$$\frac{\partial}{\partial t} mnv + \frac{\partial}{\partial z}(mnv^2 + Tn + P_{zz}) = 0, \tag{6}$$

where m is the ion mass per unit charge, v is the ion velocity along z, and P_{zz} represents radiation pressure plus the averaged, fast, electron momentum-flux

$$16\pi P_{zz} = |B|^2 + |E_y|^2 + (1-2\epsilon)|E_z|^2. \tag{7}$$

A Bernouilli-like equation

$$m\frac{\partial v}{\partial t} + \frac{\partial}{\partial z}\left(\frac{mv^2}{2} + T\ln n\right) + \frac{1}{n}\frac{\partial P_{zz}}{\partial z} = 0 \tag{8}$$

can be obtained if dissipation is neglected, when use of Eqs. (2)–(4) allows us to write the last term in (8) as a z derivative. A more detailed discussion of (2)–(8) is given in the Appendix.

Three length scales, characterizing different spatial regions, may be distinguished in system (2)–(6).

(i) Time derivatives, and dispersive and dissipative terms, can be neglected inside a reflection layer centered around $\epsilon = \sin^2\theta$, or $n = n_c\cos^2\theta$. Here, moving inward up the density profile, both $\bar{E}$ and $\bar{B}$ change from oscillatory to evanescent. The scale length is c/ω (or larger) for a radiation-to-thermal pressure ratio of order unity (or less, $\epsilon - \sin^2\theta$ then being small throughout).

(ii) Dispersive and dissipative terms must be retained in a resonance sublayer, imbedded around $\epsilon = 0$ in the reflection layer if this is not entirely subcritical. Here, a plasma wave is excited and damped as it travels outward. The scale length is λ_D [or $\lambda_D/(\Delta\epsilon_c)^{1/2}$ if the relative density change $\Delta\epsilon_c$ across the sublayer is small]. Note the nonrelativistic condition $(\lambda_D\omega/c)^2 = T/m_e c^2 \equiv \beta^2 \ll 1$; typically $\beta^2 \sim 10^{-2}$–10^{-3}.

(iii) Time derivatives must be retained in the broad region lying on both sides of the reflection layer. Here the flow adjusts to appropriate boundary conditions; it exhibits a long scale $c_s\tau_L$, c_s being $(T/m)^{1/2}$ and τ_L the laser pulse half-width, *and* the short scale of (i), due to modulation by the radiation pressure; typically $c_s\tau_L \sim 10^3 c/\omega$.

In an asymptotic analysis based on the above disparate scales, the main layer will appear as a discontinuity in the broad, external region. As it flows outward, the plasma jumps at the discontinuity from condition 4 to 1, such that $n_4 > n_c\cos^2\theta > n_1$. If there exists a resonance sublayer ($n_4 > n_c$), it will appear as a discontinuity inside the main layer, the plasma jumping from condition 3 to 2 such that $n_4 > n_3 > n_c > n_2 > n_1$ (Fig. 1).

III. STRUCTURE OF THE REFLECTION LAYER

Neglecting dispersive and dissipative terms in (4) we have

$$\epsilon E_z = B\sin\theta \tag{9}$$

and Eq. (8) becomes (see Appendix)

$$m\frac{\partial v}{\partial t} + \frac{\partial}{\partial z}\left(m\frac{v^2}{2} + T\ln n + \frac{|E_z|^2 + |E_y|^2}{16\pi n_c}\right) = 0. \tag{10}$$

Also

$$16\pi P_{zz} = \frac{\epsilon^2 + (1-2\epsilon)\sin^2\theta}{\epsilon^2}|B|^2 + \left(\frac{c}{\omega\epsilon}\frac{d|B|}{dz}\right)^2 + (8\pi S_z/c|B|)^2,$$

where S_z is the electromagnetic energy flux along z,

$$8\pi S_z \equiv \text{real part of } (-cE_y B^*), \tag{11}$$

which vanishes throughout if there is no resonance sublayer ($\epsilon_4 > 0$), but it vanishes only on its overdense side, and is constant and positive on the underdense side, if $\epsilon_4 < 0$. As we shall later see, however, due to the thinness of the sublayer

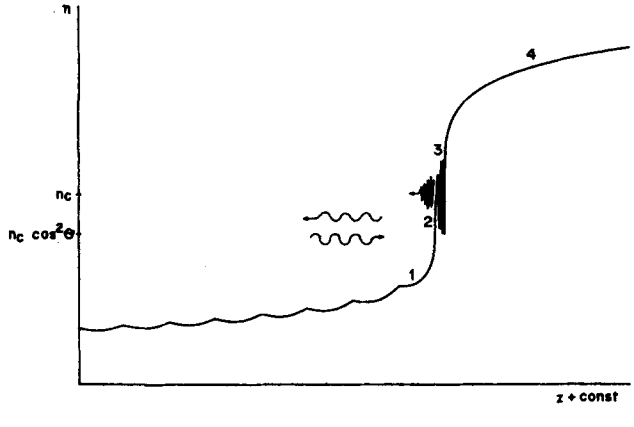

FIG. 1. Schematic density profiles for light incident at angle θ for p polarization. Note the thin reflection layer between points 4 and 1, the thinner resonance sublayer between points 3 and 2, and the rippling downstream point 1.

both the absorption fraction and S_z/cP_{zz} are of order β; here we determine the structure of the reflection layer to lowest order in β^2 by dropping S_z. Results on that structure will be used in Sec. IV to find S_z itself. Note that we may now take B, E_z, and iE_y real. At the exit 1 of the layer the field will be a standing wave; we may distinguish between condition $1m$ ($B_{1m}=0$) and $1M$ ($dB/dz|_{1M}=0$).

Next, we neglect time derivatives in (5), (6), and (10), and introduce dimensionless variables

$$\xi \equiv \frac{\omega}{c}[z - z_r(t)], \quad u \equiv \frac{-v_r}{c_s}, \quad \hat{B} \equiv \frac{B}{(16\pi n_c T)^{1/2}},$$

where z_r locates some feature of the reflection layer and $v_r = v - \dot{z}_r$. We then have $nv_r = \text{const}$ or

$$u(1-\epsilon) = u_c$$

and $mnv_r^2 + nT + P_{zz} = \text{const}$ or

$$\left(\frac{1}{\epsilon}\frac{d\hat{B}}{d\xi}\right)^2 + \frac{\epsilon^2 + (1-2\epsilon)\sin^2\theta}{\epsilon^2}\hat{B}^2 + \frac{u_c^2}{1-\epsilon} - \epsilon = \text{const}. \tag{12}$$

Also,

$$n_c(mv_r^2/2 + T\ln n) + (16\pi\epsilon^2)^{-1} \times [\hat{B}^2\sin^2\theta + (cd\hat{B}/\omega\, dz)^2] = \text{const}$$

(different on either side of the sublayer, if it exists; see Appendix). Subtracting this last equation from the momentum equation we obtain (in dimensionless form)

$$[(\epsilon - 2\sin^2\theta)/\epsilon]\hat{B}^2 + h(\epsilon, u_c) = (\text{piecewise const}), \tag{13}$$

where

$$h \equiv -\ln(1-\epsilon) - \epsilon - (u_c^2/2)[\epsilon/(1-\epsilon)]^2. \tag{14}$$

We used $u(1-\epsilon) = u_c$ in both (12) and (13).

Note here the following properties.

(a) Since

$$\frac{d\epsilon}{d\xi} \equiv \frac{2\hat{B}\, d\hat{B}/d\xi}{d\hat{B}^2/d\epsilon}, \tag{15}$$

the profile $\epsilon(\xi)$ can be obtained from Eqs. (12) and (13) by just one quadrature, if the constants, together with u_c and θ, are known; the denominator in (15) can be obtained from (13):

$$\frac{d\hat{B}^2}{d\epsilon} = \frac{\epsilon^2}{(1-\epsilon)(2\sin^2\theta - \epsilon)} \times \left[1 + 2\frac{1-\epsilon}{\epsilon^3}\hat{B}^2\sin^2\theta - \left(\frac{u_c}{1-\epsilon}\right)^2\right]. \tag{16}$$

(b) The first two terms in the above bracket add to the square of a sound speed that includes radiation pressure effects,

$$c_s^2\left(1 + 2\frac{1-\epsilon}{\epsilon}\frac{B^2\sin^2\theta}{16\pi n_c T}\right),$$

in dimensional form. At a sonic point the bracket vanishes; the profile $\epsilon(\xi)$ will remain univalued, nonetheless, if any of the conditions, $\hat{B}=0$, $d\hat{B}/d\xi = 0$, or $\epsilon = 2\sin^2\theta$, is satisfied.

(c) The entrance to the layer (subscript 4) must be subsonic according to (16): We obviously require $d|\hat{B}|^2/d\epsilon|_4 > 0$, and have $\epsilon_4 < \sin^2\theta < 2\sin^2\theta$. Also we shall make the ansatz, to be discussed in Sec. V, that the exhaust (subscript 1) is not subsonic.

(d) If the constant in (13) is $h(2\sin^2\theta, u_c)$, system (12), (13) admits as a solution, $\epsilon = \text{const} = 2\sin^2\theta$ and $\hat{B}$ variable.

A. Nonresonant regime

Consider first the case $\epsilon_4 > 0$. A single constant for (13) will be valid throughout the layer. Since we have

$$\hat{B} = \frac{d\hat{B}}{d\xi} = 0 \quad \text{at} \quad \epsilon = \epsilon_4,$$

the right-hand sides of (12) and (13) will be

$$u_c^2/(1-\epsilon_4) - \epsilon_4 \quad \text{and} \quad h(\epsilon_4, u_c),$$

respectively. According to the ansatz (c) there must exist a sonic point, where

$$1 + 2[(1-\epsilon_s)/\epsilon_s^3]\hat{B}_s^2\sin^2\theta = [u_c/(1-\epsilon_s)]^2. \tag{17}$$

At that point, (13) yields

$$[(\epsilon_s - 2\sin^2\theta)/\epsilon_s]\hat{B}_s^2 + h(\epsilon_s, u_c) = h(\epsilon_4, u_c). \tag{18}$$

Finally, according to (b) we have $d\hat{B}/d\xi|_s = 0$; we can have neither $\hat{B}_s = 0$ nor $\epsilon_s = 2\sin^2\theta$ because (17) and (18), when used in (12), would yield $(d\hat{B}/d\xi|_s)^2$ as a function of ϵ_s and ϵ_4 that can be proved negative for $0 < \epsilon_4 < \epsilon_s \leqslant 2\sin^2\theta$. We accordingly have $\epsilon_s < 2\sin^2\theta$.

Condition $d\hat{B}/d\xi|_s = 0$ in (12) reads

$$\frac{\epsilon_s^2 + (1-2\epsilon_s)\sin^2\theta}{\epsilon_s^2}\hat{B}_s^2 + \frac{u_c^2}{1-\epsilon_s} - \epsilon_s = \frac{u_c^2}{1-\epsilon_4} - \epsilon_4. \tag{19}$$

Note that points $1M$ and s coincide in the present case. Equations (17)–(19) determine ϵ_4, ϵ_s, and u_c in terms of two free dimensionless parameters, θ and $\hat{B}_{1M}^2$; it should be possible to relate $\hat{B}_{1M}^2$ to the intensity of the incident irradiation (Sec. V). The entire structure of the reflection layer may now be determined. At point $1m$ where $\hat{B}$ vanishes, ϵ is given by (13)

$$h(\epsilon_{1m}, u_c) = h(\epsilon_4, u_c). \tag{20}$$

Figure 2 shows $1 - \epsilon(\xi) \equiv n/n_c$ and $\hat{B}(\xi)$ for $\theta = 34°$ and $\hat{B}_{1M}^2 = 0.16$. The density profile exhibits weak discontinuities at the sonic points (a general feature of fluid motion).

B. Resonant regimes

1. Regime I

For fixed $\hat{B}_{1M}^2$ and θ decreasing, a value is reached beyond which ϵ_4, as given above, would be negative. This marks the appearance of resonance absorption, which takes place in a very thin sublayer. The need for a sublayer is simple to argue: If (13) were valid throughout the reflection layer for $\epsilon_4 < 0$, one would have $\hat{B} = 0$ at both $\epsilon = \epsilon_4$ and $\epsilon = 0$, $\hat{B}^2(\epsilon)$ being maximum at some intermediate $\epsilon_3 < 0$, where, according to (16), the flow should be sonic. None of the conditions of (b) above are satisfied at point 3, which would be a singular sonic point. [Equations (2), (3), and (9) lead to

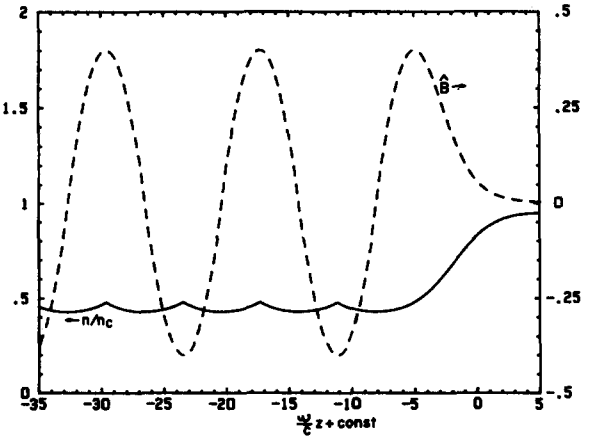

FIG. 2. Normalized density n/n_c and magnetic field $\hat{B}\equiv B/(16\pi n_c T)^{1/2}$ in the reflection layer, for $\hat{B}^2_{1M}$ (maximum $\hat{B}^2$) $= 0.16$ and $\theta = 34°$ (nonresonance regime).

$$\frac{d}{d\hat{B}^2}\left(\frac{1}{\epsilon}\frac{d\hat{B}}{d\xi}\right)^2 = \frac{\sin^2\theta - \epsilon}{\epsilon^2} > 0 \quad \text{for } \epsilon_4 \leqslant \epsilon \leqslant \epsilon_3$$

and thus $d\hat{B}/d\xi\,|_3 \neq 0$.] This would imply a multivalued solution around ϵ_3. Note, however, that as point 3 is approached, gradients become so steep that the dispersive term in (4) becomes important, invalidating Eq. (13) itself. The equation remains valid for $\epsilon_4 \leqslant \epsilon \leqslant \epsilon_3$.

At point 3 we have relations similar to (17) and (18),

$$1 + 2\frac{1-\epsilon_3}{\epsilon_3^3}\hat{E}_d^2 = \left(\frac{u_c}{1-\epsilon_3}\right)^2, \tag{21}$$

$$\left(\frac{1}{\sin^2\theta} - \frac{2}{\epsilon_3}\right)\hat{E}_d^2 + h(\epsilon_3,u_c) = h(\epsilon_4,u_c), \tag{22}$$

where we introduced $\hat{E}_d \equiv \hat{B}_3 \sin\theta$, which, as seen in Sec. IV, is the field driving the plasma wave. The sublayer may here be treated as a discontinuity imbedded in the reflection layer; an equation relating conditions at the entrance, 3, with those prevailing at the exhaust, 2, can be now derived. As before, quasisteady approximations to (5) and (6) are valid; neither nv_r nor $(mnv_r^2 + Tn + P_{zz})$ change across the discontinuity. Ignoring Eq. (4), we find that (2) and (3) yield negligible changes for B and E_y, typically of order β, so that the change of P_{zz} is only due to the last term in (7). Using (9) at point 2, where it is again valid, we obtain

$$\frac{1-2\epsilon_2}{\epsilon_2^2}\hat{E}_d^2 + \frac{u_c^2}{1-\epsilon_2} - \epsilon_2 = \frac{1-2\epsilon_3}{\epsilon_3^2}\hat{E}_d^2 + \frac{u_c^2}{1-\epsilon_3} - \epsilon_3. \tag{23}$$

Since $\hat{B} \cong$ const throughout the sublayer we can define $\hat{E}_d$ in terms of the magnetic field at $\epsilon = 0$:

$$\hat{E}_d \equiv \hat{B}_c \sin\theta.$$

Equations (21) and (23) yield a relation between ϵ_2, ϵ_3, and $\hat{E}_d$:

$$\epsilon_2 = \frac{-\epsilon_3}{1-3\epsilon_3/2}\left[1 \pm \left(1 - \frac{\epsilon_3^4}{(1-3\epsilon_3/2)^2\hat{E}_d^2}\right)^{1/2}\right]^{-1}. \tag{24}$$

Note that the upper (lower) sign in (24) corresponds to a subsonic (supersonic) velocity at 2. Here we consider the upper sign so as to recover the limit for $\epsilon_4 \to 0^+$ (no discontinuity, that is, ϵ_3 *and* ϵ_2 vanishing simultaneously). This question will be further discussed in Sec. IV.

Since 2 is subsonic, an underdense (regular) sonic point must exist as in the nonresonant regime. Equation (17) is valid at that point. Also, using (13) at both 2 and s we obtain

$$[(1/\sin^2\theta) - (2/\epsilon_2)]\hat{E}_d^2 + h(\epsilon_2,u_c) = [(\epsilon_s - 2\sin^2\theta)/\epsilon_s]\hat{B}_s^2 + h(\epsilon_s,u_c), \tag{25}$$

where the root $\epsilon_2 = \epsilon_s$ should be ignored. For ϵ_4 negative and small enough, ϵ_2 is clearly less than ϵ_s, and it must remain so throughout regime I; otherwise, point 2 would be sonic at some θ.

Finally, property (b) requires $d\hat{B}/d\xi\,|_s = 0$ so as to again recover the limit $\epsilon_4 \to 0^+$. Points s and $1M$ are therefore coincident and Eq. (19) is valid here. From (17), (19), (21), (22), (24), and (25) we obtain all quantities in terms of $\hat{B}^2_{1M}$ and θ; Eq. (20) gives ϵ_{1m} as before. Figure 3 shows $1 - \epsilon(\xi)$ and $\hat{B}(\xi)$ for $\hat{B}^2_{1M} = 0.16$, $\theta = 26°$. Note the jumps in ϵ and $d\hat{B}/d\xi$, marking the location of the sublayer.

2. Regime II

As θ is further decreased, a value is reached below which $\epsilon_s - 2\sin^2\theta$ would be positive. Below that value we drop Eq. (19) (or $d\hat{B}/d\xi\,|_s = 0$) and use

$$\epsilon_s = 2\sin^2\theta \tag{26}$$

instead, since otherwise we would obtain $\epsilon_2 < 2\sin^2\theta < \epsilon_s$, and $d\hat{B}^2/d\epsilon \propto (2\sin^2\theta - \epsilon)^{-1}$ near $\epsilon = 2\sin^2\theta$ [see Eq. (16)]; this would make $\hat{B}^2$ unbounded, in disagreement with (12). Note that the right-hand side of (25) now becomes $h(2\sin^2\theta,u_c)$, so that property (d) applies.

One now uses Eqs. (17), (21), (22), (24), (25), and (26). Actually two subregimes may be distinguished within regime II. At the higher angles, the root $\epsilon_s \neq \epsilon_2$ of (25) is used (subregime IIa). At some θ, however, (25) has a double root, and below it the root $\epsilon_s = \epsilon_2$ must be used (subre-

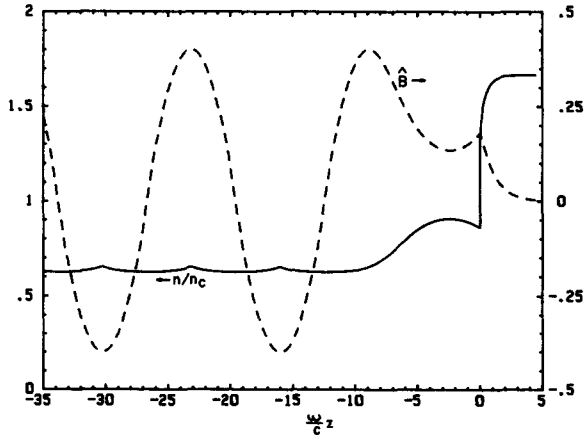

FIG. 3. Same as in Fig. 2 for $\hat{B}^2_{1M} = 0.16$ and $\theta = 26°$ (regime I); the resonance sublayer here is a discontinuity located at $z = 0$.

gime IIb); between points 2 and s, we then have $\epsilon =$ constant [property (d)].

To determine the conditions at point $1M$ (now different from point s), we use Eqs. (12) and (13), setting $d\hat{B}/d\xi\,|_{1M} = 0$:

$$\frac{\epsilon_{1M}^2 + (1-2\epsilon_{1M})\sin^2\theta}{\epsilon_{1M}^2}\hat{B}_{1M}^2 + \frac{u_c^2}{1-\epsilon_{1M}} - \epsilon_{1M} = \frac{u_c^2}{1-\epsilon_4} - \epsilon_4, \tag{27}$$

$$[(\epsilon_{1M} - 2\sin^2\theta)/\epsilon_{1M}]\hat{B}_{1M}^2 + h(\epsilon_{1M},u_c) = h(2\sin^2\theta,u_c). \tag{28}$$

Finally, using $\hat{B}_{1m}^2 = 0$ in (13), we have

$$h(\epsilon_{1m},u_c) = h(\epsilon_s,u_c) \rightarrow \epsilon_{1m} = \epsilon_s. \tag{29}$$

Throughout both IIa and IIb, we have $\epsilon =$ const between points s and $1m$ [property (d), again]. Figures 4(a) and (b) show $1-\epsilon(\xi)$ and $\hat{B}(\xi)$ for $\hat{B}_{1M}^2 = 0.16$ and $\theta = 22°$ and $\theta = 15°$, respectively. Note the flat regions in the density profiles.

3. Regime III

As θ is further decreased, a value is reached for which $\hat{B}_s^2 = 0$. At lower angles we drop (26) and use

$$\hat{B}_s^2 = 0 \tag{30}$$

instead, since a negative $\hat{B}_s^2$ would result otherwise. We now use (17), (21), (22), (24), (25), and (30). In this last equation we go back to the root $\epsilon_s \neq \epsilon_2$; in fact, we now have $2\sin^2\theta < \epsilon_2 < \epsilon_s$. For $1M$ we use (27) and (28). Points $1m$ and s are here coincident [Fig. 5(a); $\hat{B}_{1M}^2 = 0.16$, $\theta = 7°$].

Since $d\hat{B}/d\xi$, but not $\hat{B}$, changes sign across the discontinuity, $d\hat{B}^2/d\xi\,|_2$, is positive. For regimes I and IIa we also have a positive $d\hat{B}^2/d\epsilon|_2$, Eq. (16). Accordingly, Figs. 3 and 4(a) show bumps in the density profiles to the left of point 2 ($d\epsilon/d\xi\,|_2 > 0$).

The boundaries between the different regimes are marked in Fig. 6 together with $\hat{E}_d =$ const lines. For $\theta = 0$, when there is no resonance, we recover known results for normal incidence; typical profiles are given in Fig. 5(b). We note that for θ/β small, there is strictly no sublayer (profile slopes inside it are not larger than those outside); $\theta = 0$ profiles are then approximately valid throughout but a nonzero absorption should result from the usual, linear analysis,[15] using the slope at critical.

IV. STRUCTURE OF THE RESONANCE SUBLAYER

A. Proof of a subsonic 2 exit

Within the sublayer, Eq. (9) is invalid and we revert to (4) in dimensionless form,

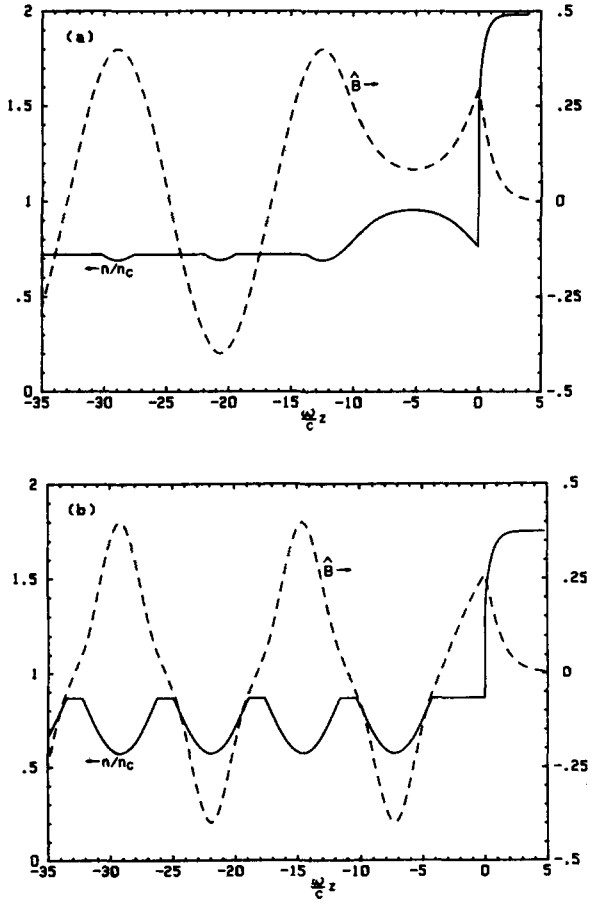

FIG. 4. Same as in Fig. 3 for $\hat{B}_{1M}^2 = 0.16$ and (a) $\theta = 22°$ (subregime IIa) and (b) $\theta = 15°$ (subregime IIb).

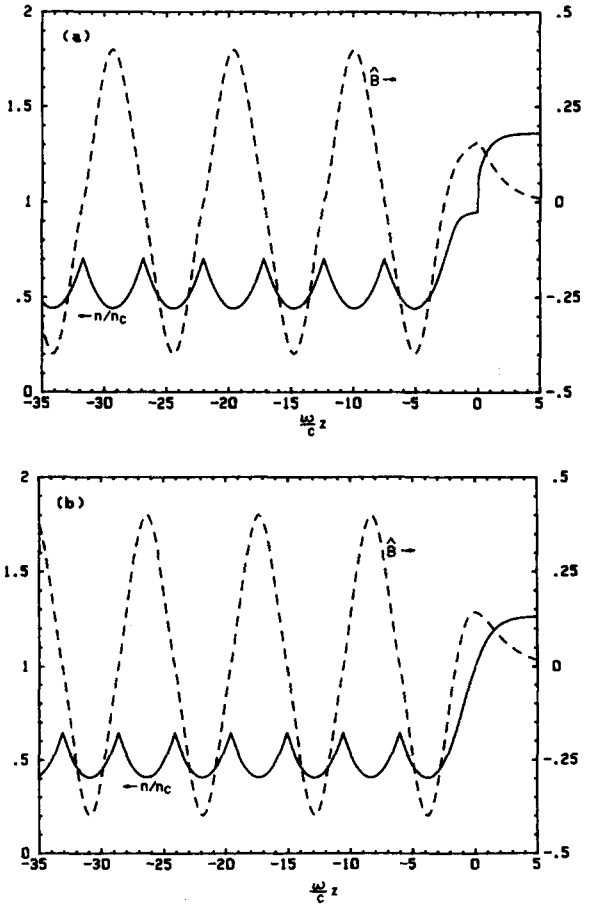

FIG. 5. Same as in Fig. 3 for $\hat{B}_{1M}^2 = 0.16$ and (a) $\theta = 7°$ (regime III) and (b) $\theta = 0°$ (normal incidence, no resonance sublayer).

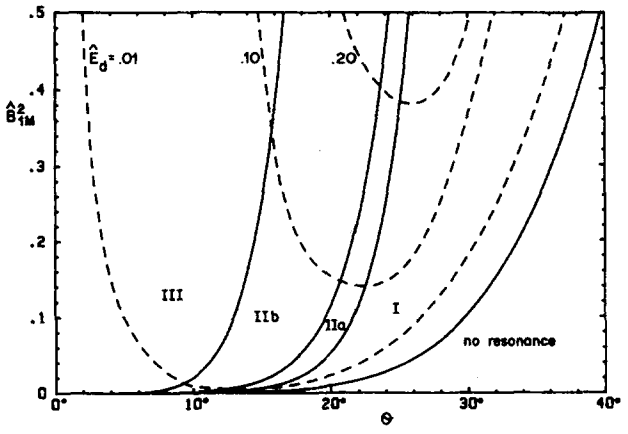

FIG. 6. Parametric plane θ-$\hat{B}^2_{1M}$ showing boundaries between regimes of the reflection layer and lines of constant normalized driver field $\hat{E}_d \equiv \hat{B}_c \sin\theta$ (— and - - -, respectively).

$$3\beta^2 \frac{d^2\hat{E}_z}{d\xi^2} + \epsilon\hat{E}_z \cong \hat{E}_d + \hat{E}_L. \tag{31}$$

Also, $\hat{P}_{zz} \equiv P_{zz}/n_c T$ in (12) must be rewritten in the general form, $|\hat{E}_y|^2 + |\hat{B}| + (1-2\epsilon)|\hat{E}_z|^2$; as noticed in Sec. III, $\hat{E}_y$ and $\hat{B}$ here are approximately constant, $-i\hat{E}_y \cong \epsilon^{-1} d\hat{B}/d\xi\,|_3$, $\hat{B} \cong \hat{E}_d/\sin\theta$, so that Eq. (12) becomes

$$\left(\frac{1}{2}-\epsilon\right)\left(|\hat{E}_z|^2 + \frac{1}{2} - \frac{u_c^2}{1-\epsilon}\right) = \left(\frac{1}{2}-\epsilon_3\right)^2\left(2\hat{E}_d^2\frac{\epsilon_3-2}{\epsilon_3^3} - 1\right) \equiv a. \tag{32}$$

Equations (31) and (32) will suffice to determine $\hat{E}_z$ and ϵ throughout the sublayer. Outside it and particularly at points 3 and 2, (31) simplifies to $\hat{E}_z = \hat{E}_d/\epsilon$; using (32) then gives back the subsonic and supersonic roots for ϵ_2 in (24), with $\epsilon_2(\text{sub}) < \epsilon_2(\text{super})$.

Note that according to (32) the sublayer, starting at $\epsilon_3 < 0$, cannot reach the value $\epsilon = \frac{1}{2}$. Now, at the lower (higher) angles in regime III (I) we find $a > 0$ and then $\frac{1}{2} < \epsilon_2$ (super) so that point 2 is necessarily subsonic, as assumed in Sec. III.

At intermediate angles, however, we have $a < 0$ and $\epsilon_2(\text{super}) < \frac{1}{2}$, and a subtler discussion is needed. It proves convenient to introduce a "sound" speed

$$c_s(1 + 2|\hat{E}_z|^2)^{1/2} \tag{33}$$

different from that considered for the reflection layer; the difference arises from the fact that at the shorter scale of the sublayer $\hat{B}$ does not change and thermal effects in (4) become important. Relative to the new sound speed, point 3 turns out to be "subsonic," root 2 (super) remaining supersonic. Hence, a point where the flow speed equals (33) must be crossed for exit 2 to be supersonic. The "sonic" condition $d|\hat{E}_z|^2/d\epsilon = 0$ together with (32) yields

$$\epsilon(\text{sonic}) = \frac{|a|^{1/2} - u_c/2}{|a|^{1/2} - u_c}, \tag{34}$$

$$|\hat{E}_z|^2(\text{sonic}) = 2(|a|^{1/2} - u_c)^2 - \tfrac{1}{2}; \tag{35}$$

in addition, we must have $d|\hat{E}_z|^2/d\xi = 0$ at sonic, since otherwise $\epsilon(\xi)$ would be multivalued.

Using $\epsilon(|\hat{E}_z|^2)$ from (32), Eq. (31) is analogous to the equation of an elastic pendulum of coordinates, the real and imaginary parts of $\hat{E}_z$, with damping, a nonlinear tension, and gravity (which points along the positive Re $\hat{E}_z$ axis).

For negligible damping, Eq. (31) has a first integral ("energy")

$$3\beta^2\left|\frac{d\hat{E}_z}{d\xi}\right|^2 + V[\epsilon(|\hat{E}_z|^2)] - 2\hat{E}_d \,\text{Re}\,\hat{E}_z = \text{const}, \tag{36}$$

$$V(\epsilon) \equiv \frac{u_c^2\epsilon}{1-\epsilon} + \frac{2a\epsilon}{1-2\epsilon} + \ln\left[(1-\epsilon)^{u_c^2}(1-2\epsilon)^a\right]; \tag{37}$$

with damping, the energy will decrease with decreasing ξ. Now, leaving the sublayer, at point 3, we have $3\beta^2|d\hat{E}_z/d\xi|^2 \cong 0$ and one easily finds that if

$$(V - 2\hat{E}_d|\hat{E}_z|)_{\text{sonic}} > V(\epsilon_3) - 2\hat{E}_d^2/\epsilon_3, \tag{38}$$

then the sonic point cannot be reached, and the exit 2 is again necessarily subsonic; (38) is a *conservative* condition. Using an equal sign in (38), and Eqs. (34) and (35), we obtain two lines in the θ-$\hat{B}^2_{1M}$ plane marked in Fig. 7. Outside the region within the lines, we can be sure that point 2 *is* subsonic, as assumed in Sec. III. For conditions inside, further analysis is required; we exclude that region from the present study. Note that as one enters this region, $1 - u_c^2$ becomes small; it can be shown that nonquasineutral effects then need to be considered, making the analysis more difficult.

Takabe and Mulser[11] analyzed the sublayer using (31), and a Bernoulli-like equation instead of (32), considering that its exhaust had to be supersonic; they discussed values of $\hat{E}_d$ of order unity and used an *ad hoc* expression for E_L. Kruer[12] carried out a similar analysis, though he only studied small $\hat{E}_d$ and avoided choosing a Landau damping model by introducing at some stage a linear approximation for ϵ.

B. Low driver limit

For $1 - u_c^2 = O(1)$ and driver $\hat{E}_d$ small, Eqs. (31) and (32) give scaling laws

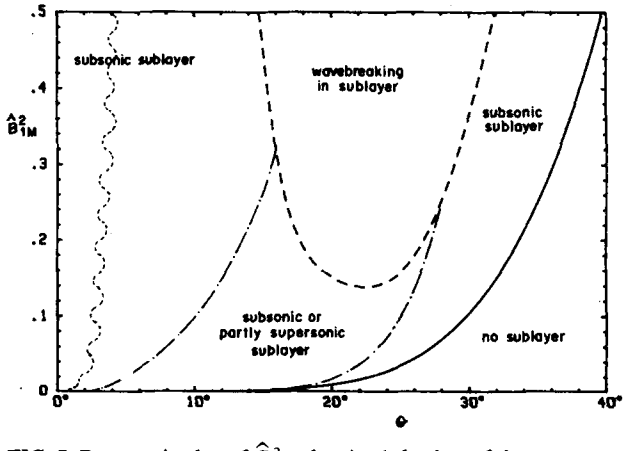

FIG. 7. Parametric plane θ-$\hat{B}^2_{1M}$ showing behaviors of the resonance sublayer. The dashed line ($\hat{E}_d = 0.1$) is a rough boundary for wave breaking. Nonquasineutral effects become important as one enters the region between the dash–dotted lines. To the left of the wavy line, a quasilinear analysis of the sublayer is valid.

thickness layer $\Delta\xi \sim \beta \hat{E}_d^{-1/3}$,

$\epsilon \sim |\hat{E}_z|^2 \sim \hat{E}_d^{2/3}$,

so that both ϵ and $|\hat{E}_z|$ become of order unity with $\hat{E}_d$. From the fast momentum equation for electrons one easily finds that if $|\hat{E}_z| = O(1)$, then $(v_{eh})_z^2 \cong T/m_e$ and wavebreaking occurs (see Appendix). Thus, in order to avoid wavebreaking, we hereafter assume $\hat{E}_d$ small for the analysis of the sublayer. We can roughly say that the analysis is valid below the line $\hat{E}_d = 0.1$, marked in Fig. 7.

Linearizing Eq. (32) and using $1 - u_c^2 \cong -2\hat{E}_d^2/\epsilon_3^3$ from (21), we obtain

$$\epsilon = |\hat{E}_z|^2/(1-u_c^2) + \tfrac{3}{2}\epsilon_3. \tag{39}$$

Introducing next

$$\tau \equiv \beta^{-1}(-\epsilon_3/3)^{1/2}\xi, \quad R \equiv -\epsilon_3 \hat{E}_z/\hat{E}_d, \tag{40}$$

Eqs. (31) and (39) yield

$$\frac{d^2R}{d\tau^2} + \frac{|R|^2-3}{2}R = 1 + \frac{\hat{E}_L}{\hat{E}_d}, \quad R = X + iY.$$

The solution to the above equation, for τ large and negative, must represent (i) a progressively damped, outgoing plasma wave, and (ii) no incoming plasma wave. The solution would yield the absorbed flux; naturally, a definite expression for E_L would be required. However, if $\hat{E}_L/\hat{E}_d$ is small enough, the absorption is independent of E_L and can be computed with no regard for its value: Taking into account the slow changes of both $\hat{E}_y$ and $\hat{B}$ within the sublayer allows us to determine the outgoing energy flux $-S_{z,a}$, which should be ultimately absorbed over a larger distance.

Defining

$$\mathscr{E} \equiv i\epsilon_3 \hat{E}_y/\hat{E}_d, \quad b \equiv \hat{B}\sin\theta/\hat{E}_d,$$

Eqs. (2) and (3) become

$$\frac{d\mathscr{E}}{d\tau} = \beta\sigma\left(3R - \frac{b}{\sigma^2}\right), \tag{41}$$

$$\frac{db}{d\tau} = \frac{3}{2}\beta\sigma\mathscr{E}(|R|^2 - 3 + |\mathscr{E}|^2 - \mathscr{E}_3^2), \tag{42}$$

where the parameters

$$\sigma^2 \equiv \frac{\sin^2\theta}{3|\epsilon_3|}, \quad \mathscr{E}_3 \equiv \frac{-1}{\sin\theta}\frac{d\ln\hat{B}}{d\xi}\bigg|_3$$

are known functions of θ and $\hat{B}_{1M}^2$. We have included changes of $|\hat{E}_y|^2$ in the momentum equation (39); changes of $|\hat{B}|^2$ are smaller by a factor $|\epsilon_3|$, at least. For R we now have

$$\frac{d^2R}{d\tau^2} + \frac{|R|^2 - 3 + |\mathscr{E}|^2 - \mathscr{E}_3^2}{2}R = b. \tag{43}$$

1. Small angles

For θ small, we have $\sigma^2, \mathscr{E}_3^{-1} \ll 1$. A change $\Delta|\mathscr{E}|^2 = O(1)$ then occurs over a distance

$$\Delta\tau \sim \sigma|\Delta\mathscr{E}|/\beta \sim \sigma/\beta\mathscr{E}_3.$$

For such a range we have

$$\Delta b \sim \sigma^2, \quad b \cong 1.$$

Freely choosing $\xi_3 = 0$, system (41)–(43) then yields

$$\frac{d^2R}{d\tau^2} + \frac{1}{2}(|R|^2 - 3 - 2\delta\tau)R = 1, \quad \delta \equiv \frac{\beta\mathscr{E}_3}{\sigma}. \tag{44}$$

For $\delta \gg 1$ (θ small enough), the nonlinear term in ϵ has a negligible effect, and we end with the well-known, linear warm-plasma limit. In this case there is strictly no sublayer, as noticed at the end of Sec. III. The solution to (44), retaining just the linear term inside the bracket, may be written, as usual, as a combination of Airy functions Ai and Gi,[16] and one obtains

$$\frac{-S_{z,a}}{2cn_cT} \equiv -\hat{S}_{z,a} = \frac{\pi\beta\hat{E}_d^2}{|\epsilon_3|^{3/2}}\frac{3^{1/2}}{\delta}. \tag{45}$$

Since $|\epsilon_3|^{3/2} \sim \hat{E}_d$, and both $\hat{E}_d$ and $\sigma/\mathscr{E}_3$ grow with θ, $|\hat{S}_{z,a}|$ grows with increasing angle. For δ of order unity, a numerical analysis is required. Equation (44) was previously considered by Morales and Lee,[8] Gil'denburg and Fraiman,[9] and Adam *et al.*[10] In all cases it was assumed that

$$\epsilon = |\hat{E}_z|^2 - z/L + \text{const};$$

the scale length L was arbitrary, and motion was ignored. In our analysis we have from (39), with the $\Delta|\hat{E}_y|^2$ term,

$$\epsilon = (1-u_c^2)^{-1}|\hat{E}_z|^2 - z/L + \text{const},$$

$\omega L/c$ being self-consistently obtained in terms of θ and $\hat{B}_{1M}^2$ from the results of Sec. III,

$$(\omega/c)L = \sin\theta(1-u_c^2)/2\hat{E}_d|\hat{E}_{y3}|.$$

Equation (45) then takes the usual form $-\hat{S}_{z,a} = \pi\hat{E}_d^2\omega L/c$. There was no reflection-layer analysis in Refs. 8–10.

For δ small, the numerical results of Gil'denburg and Fraiman, written in our variables, take the form

$$-\hat{S}_{z,a} \cong (\pi\beta\hat{E}_d^2/|\epsilon_3|^{3/2}) \times 1.54. \tag{46}$$

Using a simple WKB model they also found 2.31 instead of factor 1.54. Adam *et al.* found numerically

$$-\hat{S}_{z,a} \cong (\pi\beta\hat{E}_d^2/|\epsilon_3|^{3/2}) \times 2.61\delta^{0.8},$$

for $2 < \delta^{-1} < 14$. (Morales and Lee only considered δ large and unsteady effects.)

Actually, for δ small (but σ^2 still small), Eq. (44) exhibits two τ scales, allowing some simplifications. First, the boundary conditions for $\tau \to +\infty$ are now clear: Leaving the sublayer on the overdense side, $-R$ must be near unity [$Y^2 + (X+1)^2 \ll 1$] and (44) gives

$$\frac{d^2Y}{d\tau^2} \cong Y \quad \text{or} \quad Y \cong e^{-\tau} \times \text{const}, \tag{47}$$

the constant being determined from the condition that there is no incoming plasma wave for $-\tau$ large; it also gives

$$\frac{d^2f}{ds^2} - f^2 \cong -s, \tag{48}$$

with

$$s \equiv (3\delta/2)^{1/5}\tau, \quad f \equiv (27/8\delta^2)^{1/5}(X+1). \tag{49}$$

The solution to (48) with R decreasing into the outer layer is $f \cong s^{1/2} - (8s^2)^{-1}$ for $s \gg 1$, and $f \cong 6s^{-2} + s^3/6$ for $s \ll 1$, condition $X + 1 \ll 1$ then requiring $s \ll \delta^{-4/5}$ and $s \gg \delta^{1/5}$, respectively. Thus, for moderately large τ, we have

$$X \cong -1 + 4/\tau^2 + \delta\tau^3/6 + \cdots, \quad 1 \ll \tau \ll \delta^{-1/5}. \tag{50}$$

Secondly, going back to the analogy with a pendulum, the time dependence of the tension can now be handled in an approximate way. The energy of the pendulum

$$U \equiv \frac{1}{2}\left|\frac{dR}{d\tau}\right|^2 + \frac{1}{8}|R|^4 - \frac{3}{4}|R|^2 - X \tag{51}$$

obeys the equation

$$\frac{d}{d\tau}\left(U - \frac{\delta}{2}\tau|R|^2\right) = -\frac{\delta}{2}|R|^2 \tag{52}$$

while the "angular momentum" is determined by

$$\frac{d}{d\tau}\left(X\frac{dY}{d\tau} - Y\frac{dX}{d\tau}\right) = -Y \tag{53}$$

and is directly related to the energy flux of the outgoing plasma wave

$$-\hat{S}_{z,a} = \frac{\pi\beta\hat{E}_d^2}{|\epsilon_3|^{3/2}}\frac{3^{1/2}}{\pi}\left(X\frac{dY}{d\tau} - Y\frac{dX}{d\tau}\right).$$

Note that though R and angular momentum change in a scale $\Delta\tau \sim 1$, $U - \delta\tau|R|^2/2$ requires a longer scale $\Delta\tau \sim \delta^{-1}$; the slow variation of this last quantity will be now approximately determined in an average way.

We consider

$$\Omega^2 \equiv \tfrac{1}{2}(|R|^2 - 3 - 2\delta\tau)$$

in Eq. (44) as a slowly changing function $\Omega(\delta\tau)$; this leads to a WKB solution

$$R = \Omega^{-2} + C\Omega^{-1/2}\exp\left(-i\int_0^\tau \Omega(\delta\tau')d\tau'\right). \tag{54}$$

Then we have

$$\left\langle X\frac{dY}{d\tau} - Y\frac{dX}{d\tau}\right\rangle = C^2 = \text{const}$$

in agreement with the average of (53), and

$$\langle U\rangle = \frac{C^2\Omega}{2} + \frac{1}{8\Omega^8} + \frac{C^2}{2\Omega^5} + \frac{C^4 - 8}{4\Omega^4} - \frac{3}{4\Omega^4} - \frac{3C^2}{4\Omega}; \tag{55}$$

while Eq. (52) yields

$$\delta\tau = -\frac{d\langle U\rangle/d\Omega}{d\langle|R|^2\rangle/d\Omega} \equiv \frac{3}{4} + \frac{2C^2\Omega^3(\Omega^6 - 5) - \Omega^6(C^4 - 8) - 4}{4\Omega^4(4 + C^2\Omega^3)}. \tag{56}$$

At $\delta\tau$ small we have $\langle U\rangle = U$, and taking $R \cong -1$, $dR/d\tau \cong 0$ from (47) and (50), Eq. (51) gives a value $\langle U\rangle = \frac{3}{8}$, which, used in (55), yields one relation between C and $\Omega(0)$. A second relation is provided by Eq. (56). We thus finally obtain

$$C^2 \cong 3.23, \quad \Omega(0) \cong 1.10, \tag{57}$$

$$-\hat{S}_{z,a} \cong (\pi\beta\hat{E}_d^2/|\epsilon_3|^{3/2}) \times 1.78, \tag{58}$$

in good agreement with (46).

2. Large angles

At the larger angles, we have $\sigma \gtrsim O(1)$, and system (41)–(43) retains all its complexity. However, as long as $\sigma\beta$ is small (that is, except in a very thin region next to the nonresonance boundary), Eqs. (41) and (42) again introduce a slow scale into (43). Accordingly, boundary conditions at the entrance of the sublayer take the same form as Eqs. (47) and (50), with $\delta(1 + 6\sigma^2)$ instead of δ; and using the preceding average approach, approximating R by Eq. (54), one recovers results (57) and (58).

We have thus determined the normalized absorbed flux as a function of θ and $\hat{B}_{1M}^2$ throughout the resonance region of Fig. 7, the result being strictly valid if $\hat{E}_d$ is small and point 2 subsonic. Equation (58) applies everywhere, except at very small angles, when (45) is valid; for $\beta = 0.05$ these angles lie, roughly, at the left of the wavy line of Fig. 7.

V. FLOW STRUCTURE OUTSIDE THE REFLECTION LAYER

A. Absorption coefficient

As noticed at the end of Sec. II, the flow in the broad region past the reflection layer exhibits both the long scale of the overall corona and the short scale of rippling due to radiation pressure. If there was no rippling, a WKB approximation would adequately describe the wave field; the electromagnetic energy flux incident on the layer at point 1 would be given by Eq. (11), that is,

$$\hat{S}_{z,i} = \tfrac{1}{4}|\hat{B}_{1M}||\hat{E}_{y1m}| \tag{59}$$

$$= [(\epsilon_1 - \sin^2\theta)^{1/2}/4\epsilon_1]|\hat{B}_{1M}|^2. \tag{60}$$

Here, $\hat{B}_{1M}$ and $\hat{E}_{y1m}$ are values at the maximum and minimum of the magnetic field, respectively, ϵ taking a nearly constant value, ϵ_1, in the short scale.

When there is rippling, the WKB analysis fails and formulas (59) and (60) are not strictly valid. Use of either one in some appropriate way may be, however, a reasonable approximation. Here we shall use formula (59). Note that $\hat{B}_{1M}$ and $\hat{E}_{y1m}$ are still well defined, while ϵ_1 in (60) is not; a value $(\epsilon_{1M} + \epsilon_{1m})/2$ was used by Lee *et al.*[2] for the simple case of normal incidence. (For a more rigorous analysis see Sanmartín and Montañés[17].)

Using $-S_{z,a}$ as the net energy flux at point 1, the fractional absorption $A = -\hat{S}_{z,a}/\hat{S}_{z,i}$ is given by

$$\frac{A}{\beta} = \frac{\pi\hat{E}_d^2/|\epsilon_3|^{3/2}}{|\hat{B}_{1M}||\hat{E}_{y1m}|/4}\, g(\delta), \tag{61}$$

with $\delta \equiv \beta\mathscr{C}_3/\sigma$ and

$$g \cong 3^{1/2}/\delta, \quad \text{for} \quad \delta \gg 1,$$

$$g \cong 1.78, \quad \text{for} \quad \delta \ll 1.$$

For $\delta \ll 1$, the right-hand side of (61) is a function of θ, $\hat{B}_{1M}^2$, and is given in Fig. 8. For θ small enough ($\delta \gg 1$), A, but not A/β, is a function of θ, $\hat{B}_{1M}^2$.

B. Outer flow structure

To now determine the structure of the outer region in the long scale, we go back to Eqs. (5) and (6). On the denser side, and if T is independent of z (thermal wave regime), a self-similar solution exists[6]; here we shall assume that T is also independent of time.[18] We shall also assume that some

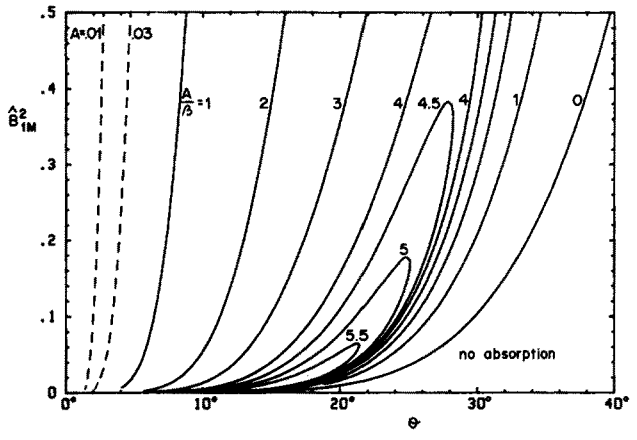

FIG. 8. Fractional absorption A as a function of θ, $\hat{B}^2_{1M}$, and $\beta = (T/m_e c^2)^{1/2}$. For very small θ (quasilinear sublayer) A is independent of β.

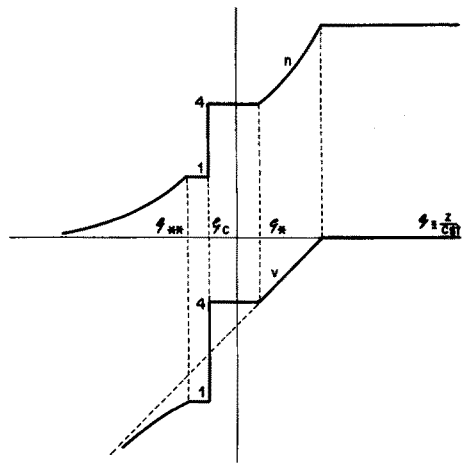

FIG. 9. Density and velocity profiles in the approximate self-similar solution for the isothermal corona outside the reflection layer (here represented as a discontinuity). Note the plateaus joining the different types of solutions.

average $\langle \hat{P}_{zz} \rangle$ can be written down as a function of just ϵ in the underdense side. Then, defining

$$\zeta \equiv z/c_s t, \quad w \equiv v/c_s,$$

Eqs. (5) and (6) take a self-similar form

$$(\zeta - w)\frac{d}{d\zeta}\ln(1-\epsilon) = \frac{dw}{d\zeta}, \tag{62}$$

$$\left(1 - \frac{d\langle \hat{P}_{zz}\rangle}{d\epsilon}\right)\frac{d}{d\zeta}\ln(1-\epsilon) = (\zeta - w)\frac{dw}{d\zeta}. \tag{63}$$

These equations admit two types of solutions, (i)

$$\frac{dw}{d\zeta} = 0, \quad \frac{d\epsilon}{d\zeta} = 0, \tag{64}$$

and (ii)

$$\zeta - w = \left(1 - \frac{d\langle \hat{P}_{zz}\rangle}{d\epsilon}\right)^{1/2}, \tag{65a}$$

$$\int \left(1 - \frac{d\langle \hat{P}_{zz}\rangle}{d\epsilon}\right)^{1/2} d\ln(1-\epsilon) - w = \text{const}. \tag{65b}$$

On the dense side we clearly recover the known results, (64) and

$$\zeta - w = 1, \quad \ln(1-\epsilon) - w = \text{const}. \tag{66}$$

The entire outer structure resulting from (64), and (65) or (66), is shown in Fig. 9. To the right, we have the undisturbed medium for $\zeta > 1$ ($w = 0$, $\epsilon = \epsilon_0 \equiv 1 - n_0/n_c$, n_0 being the target density). Next, there is a region where (66) applies

$$w = \zeta - 1, \quad 1 - \epsilon = (1 - \epsilon_0)e^{\zeta - 1};$$

note the weak discontinuity at $\zeta = 1$, advancing into the undisturbed target at the thermal sound speed c_s. At some point ζ_*, a second weak discontinuity exists where one switches to a solution of type (64); using ϵ_4 as given in Sec. III we obtain ζ_* and w_*,

$$1 - \epsilon_4 = (1 - \epsilon_0)e^{\zeta_* - 1}, \quad w_* = \zeta_* - 1.$$

The plateau ($w = \text{const}$, $\epsilon = \text{const}$) extends from ζ_* to ζ_c, with entrance to the discontinuity represented by the reflection layer (including the resonance sublayer if it exists). From the definition in Sec. III we have $u = \zeta_c - w$ at the discontinuity; we then find

$$w_4 = w_*, \quad u_4 = u_c/(1 - \epsilon_4), \quad \zeta_c = u_4 + w_4.$$

Using some average value $\langle \epsilon_1 \rangle$ we obtain

$$\langle u_1 \rangle = u_c/(1 - \langle \epsilon_1 \rangle), \quad w_1 = \zeta_c - \langle u_1 \rangle.$$

A second plateau [solution of type (64)] extends to a value ζ_{**} where (65) applies

$$\zeta_{**} - w_1 = \left(1 - \frac{d\langle \hat{P}_{zz}\rangle}{d\epsilon}\bigg|_{\langle \epsilon_1 \rangle}\right)^{1/2}.$$

Equation (65) is now valid for $-\infty < \zeta < \zeta_{**}$, completing the solution.

We finally prove ansatz (c) of Sec. III. Note that for the solution to be univalued, one must have $\zeta_c > \zeta_{**}$, or

$$\langle u_1 \rangle^2 > 1 - \frac{d\langle \hat{P}_{zz}\rangle}{d\epsilon}\bigg|_{\langle \epsilon_1 \rangle}. \tag{67}$$

We now choose a definite mean $\langle \hat{P}_{zz} \rangle$. Using the WKB approximation, as if there was no rippling, one obtains

$$\hat{P}_{zz} = 4\hat{S}_{z,i}/\epsilon(\epsilon - \sin^2\theta)^{1/2} \times \left[\epsilon - \sin^2\theta + (2\sin^2\theta - \epsilon)(1-\epsilon) \times \cos^2\left(\frac{\omega}{c}\int^z (\epsilon - \sin^2\theta)^{1/2}\, dz'\right)\right];$$

we define $\langle \hat{P}_{zz} \rangle$ by just using $\frac{1}{2}$ for the squared cosine above,

$$\langle \hat{P}_{zz} \rangle = [2(\epsilon + \cos 2\theta)/(\epsilon - \sin^2\theta)^{1/2}]\hat{S}_{z,i}.$$

Also,

$$\langle \hat{B}^2 \rangle = 2\hat{S}_{z,i}\epsilon(\epsilon - \sin^2\theta)^{-1/2},$$

so that (67) becomes

$$1 + \frac{(1 - \langle \epsilon_1 \rangle)\langle \hat{B}_1^2 \rangle}{2\langle \epsilon_1 \rangle(\langle \epsilon_1 \rangle - \sin^2\theta)} - \langle u_1 \rangle^2 < 0.$$

A comparison to the bracket in Eq. (16) shows that if the

above condition is satisfied $\langle u_1 \rangle$ must be supersonic when the sound speed of Sec. III is used.

VI. DISCUSSION OF THE RESULTS

We have considered the isothermal thin region around critical density n_c, in the corona of a laser target, where the pressure of the light steepens the plasma profile. The light of wavelength $\lambda(n_c)$ impinges on the stratified flow at angle θ and p polarization. One may distinguish (i) a reflection layer, where the wave field turns from oscillatory to evanescent, and (ii) an imbedded sublayer where resonance absorption occurs. We studied the wave equations, with a cold dielectric function and thermal, dispersive effects (collisions neglected), and the low-frequency, quasineutral continuity and total momentum equations, including the radiation pressure with high-frequency averaged terms.

The structure of the reflection layer shows a variety of behaviors, which have been fully determined in terms of both angle θ and peak magnetic pressure (normalized to the thermal pressure at critical) $\hat{B}^2_{1M}$. Both thermal effects in the wave equations and absorption effects (which are small because of the thinness of the resonance sublayer) are neglected here. One can define an effective sound speed that includes a radiation pressure term. The high-density entrance to the layer (point 4) was then proved to be subsonic, while for the low-density exhaust (point 1) we made the ansatz that it is not subsonic. For given $\hat{B}^2_{1M}$ and large enough θ the entire layer is underdense and crossing a regular sonic point, where the magnetic field is maximum, determines the structure. The critical surface will lie somewhere in the unsteepened plasma on the denser side of the layer, giving rise to a negligible, exponentially small, absorption.

For smaller angles point 4 is overdense and the layer develops a discontinuity, overdense on one side where the flow has a singular sonic point (point 3). Jump conditions at the discontinuity show that the underdense side (point 2) may be either subsonic or supersonic; in the first case, considered here, there must be a regular sonic point between 2 and 1, again allowing a full determination of the structure. There are now three different regimes (Fig. 6). The regular sonic point occurs at a maximum of the magnetic field for the larger angles (regime I), and at a minimum (zero), as in the case of normal incidence, for the lower angles (regime III). For intermediate incidence (regime II), the regular sonic point occurs at a value of the dielectric function $(1 - n/n_c)$ equal to $2 \sin^2 \theta$; actually two subregimes may then be distinguished. Fluid profiles show bumps, weak discontinuities, and plateaus. Finally, the energy flux incident on the layer is determined using some WKB approximation at its exhaust.

The structure of the resonance sublayer (the discontinuity when analyzed in a finer scale) was determined for the case of small $3 \rightarrow 2$ jumps. This avoids the problem of wave breaking within the sublayer and requires that $\hat{E}_d$ (the normalized driver field of capacitor models, $\hat{B}_c \sin \theta$) be small; Fig. 7 shows the curve of the θ-$\hat{B}^2_{1M}$ plane where $\hat{E}_d = 0.1$. It was proved that except inside a region, marked in the same figure, point 2 was necessarily subsonic, as previously assumed; inside that region, nonquasineutral effects make it difficult to ascertain whether point 2 is subsonic or supersonic.

Determining the absorption requires a knowledge of Landau damping for a nonlinear, inhomogeneous fluid evolution, unless the damping is small enough, when taking into account the slow variation of magnetic and transverse electric fields within the sublayer provides a large, self-consistent scale length and allows computation of the outgoing energy flux of the plasma wave and thus the absorption. For θ small enough, it suffices to determine the slope of the density profile at critical and use known results on absorption for a linear profile. For all other angles we used an analytical averaging approximation that compares well with the numerical results of Gil'denburg and Fraiman[9] for a similar equation.

A basic difference between our work and that of other researchers[9-12] is that they did not carry out an analysis of the reflection layer, which is required for a self-consistent determination of absorption. Note, in addition, that in Refs. 9 and 10 the relation between the dielectric function and radiation pressure was a static one, and the scale length at critical was a free parameter; in Refs. 11 and 12, point 2 was assumed to be always supersonic, and either Landau damping or the scale length was fixed in some crude way.

The broad, overall flow on either side of the reflection layer was assumed to be isothermal. A WKB approximation that averaged the short-scale rippling due to radiation pressure was used for the region downstream of the layer leading to a self-similar solution; this allowed us to prove the ansatz that its exhaust was not subsonic.

Figure 10 shows the fractional absorption for given $T/m_e c^2$, θ, and $I\lambda^2/T$; we have used $I\lambda^2/T$ (I = intensity, T = electron temperature), which is proportional to the normalized, light energy-flux reaching the reflection layer, as a free parameter instead of $\hat{B}^2_{1M}$. Actually, for θ small enough, the absorption is independent of $T/m_e c^2$.

Figure 11 shows the densities at entrance and exhaust of both the reflection layer (points 4 and 1) and resonance sublayer (points 3 and 2). Note the complex dependence of the curves on both θ and $I\lambda^2/T$. Comparison of Fig. 11 with

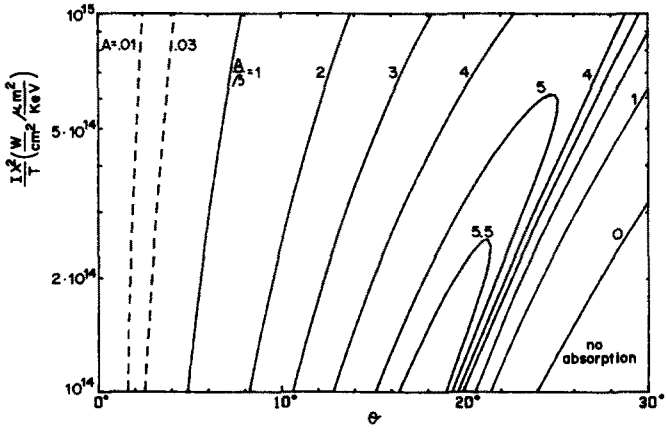

FIG. 10. Fractional absorption A as a function of θ, β, and $I\lambda^2/T$; I is the intensity reaching the reflection layer, λ the wavelength, and T the local electron temperature.

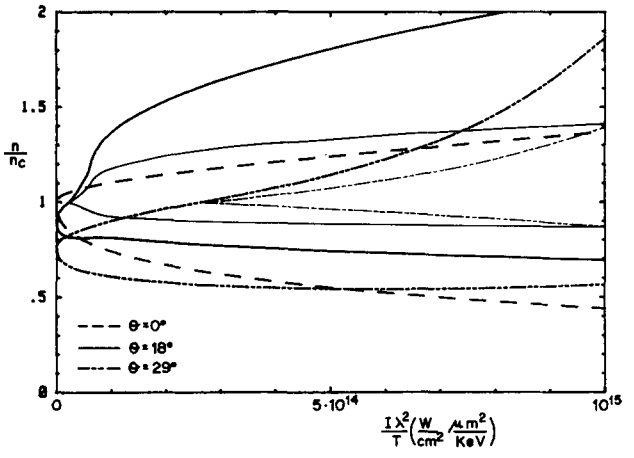

FIG. 11. Densities at the entrance and exhaust of the reflection layer versus $I\lambda^2/T$ for several angles. Because of the rippling, the lower (exhaust) lines are averaged values. Also shown (thin lines) are densities at the entrance and exhaust of resonance sublayer, starting when the entrance to the reflection layer reaches the critical density.

published data from experiments or simulations [19] was not possible because either they correspond to a wave-breaking regime, or data were lacking (in particular θ).

Present results could be of use in simulation codes, which would avoid considering the complex steepened region. Naturally, an analysis (now in progress) that would include both p- and s-polarized light in the reflection layer would be of greater interest.

ACKNOWLEDGMENT

This research was supported by the Comisión Interministerial de Ciencia y Tecnologia of Spain (PB87 0569).

APPENDIX: DISCUSSION OF THE BASIC EQUATIONS

The high-frequency part of the electron momentum equation yields the usual quivering velocity

$$\bar{v}_{eh} = (-ie/m_e\omega)[\bar{E} - (n_c/n)\bar{F}]; \tag{A1}$$

$\bar{F}$ includes a dispersive term, where Poisson's equation is used, and some model term $\bar{E}_L$ for Landau damping:

$$\bar{F} = 3\lambda_D^2 \nabla(\nabla\cdot\bar{E}) - \bar{E}_L. \tag{A2}$$

Maxwell's equations then take the form

$$\nabla\wedge\bar{E} = i(\omega/c)\bar{B}, \quad \epsilon = 1 - n/n_c, \tag{A3}$$

$$\nabla\wedge\bar{B} = -i(\omega/c)(\epsilon\bar{E} + \bar{F}). \tag{A4}$$

To obtain $\bar{v}_{eh}$ we assumed that the convective term in the momentum equation was negligible, $|\bar{v}_{eh}\cdot\nabla\bar{v}_{eh}| \ll |\partial\bar{v}_{eh}/\partial t|$ or, using (A1),

$$|\bar{v}_{eh}| \sim |\bar{E}|(n_c m_e)^{-1/2} \ll \omega\times\text{scale length}; \tag{A5}$$

in this case there is no wave breaking and the high-frequency current density is $\bar{J}_h = -en\bar{v}_{eh}$.

For the reflection layer, and a nonrelativistic plasma, the assumption is satisfied for $|\bar{E}|^2/n_c T \leqslant O(1)$, because the scale length is no less than c/ω. For the resonance sublayer, where we require that the dispersive term in (A4) be dominant, $F_z \sim \epsilon E_z$, use of (A2) gives a scale length $\lambda_D/\Delta\epsilon_c^{1/2}$, with $\Delta\epsilon_c$ some characteristic value. Condition (A5) then becomes $\Delta\epsilon_c|E_z|^2/n_c T \ll 1$. Since the low-frequency total momentum equation gives $\Delta\epsilon_c \sim |E_z|^2/n_c T$ (Sec. IV), wave breaking is avoided only if $\Delta\epsilon_c$ is small (and thus we have $|\bar{F}| \ll |\bar{E}|$ everywhere). Equations (A3) and (A4) then give system (2)–(4) as a valid approximation for both layer and sublayer.

The general form of the low-frequency total momentum equation, $mn(\partial\bar{v}/\partial t + \bar{v}\cdot\nabla\bar{v}) = -\nabla(nT) - \nabla\cdot\bar{\bar{P}}_r$, involves the radiation pressure[20]

$$\bar{\bar{P}}_r \equiv \left\langle \frac{E^2+B^2}{8\pi}\bar{\bar{I}} - \frac{\bar{E}\bar{E}+\bar{B}\bar{B}}{4\pi}\right\rangle + \langle m_e n\bar{v}_{eh}\bar{v}_{eh}\rangle$$
$$\cong \left\langle \frac{E^2+B^2}{8\pi}\bar{\bar{I}} - \frac{\epsilon\bar{E}\bar{E}+\bar{B}\bar{B}}{4\pi}\right\rangle - \langle\bar{E}\bar{F}+\bar{F}\bar{E}\rangle,$$

where the fields are now real and we have indicated the high-frequency averages and neglected terms quadratic in $\bar{F}$. For irrotational flow (as in the case of a one-dimensional thin layer) we obtain, *using Eqs. (A3) and (A4)*,

$$-\frac{\partial}{\partial t}m\bar{v} = \nabla\frac{mv^2}{2} + \frac{1}{n}\nabla(Tn) + \frac{1}{n}\nabla\cdot\bar{\bar{P}}_r, \tag{A6a}$$

$$\frac{1}{n}\nabla\cdot\bar{\bar{P}}_r \cong \nabla\frac{\langle E^2\rangle}{8\pi n_c} - \nabla\cdot\frac{\langle\bar{E}\bar{F}\rangle}{4\pi n_c} - \frac{\langle\nabla\bar{E}\cdot\bar{F}\rangle}{4\pi n_c}. \tag{A6b}$$

Without radiation pressure (A6) is the usual Bernoulli equation if the flow is isentropic[18] (its right-hand side then being the gradient of total enthalpy per electron), and a similar equation if the flow is isothermal (the quantity under the gradient being the total Gibbs free energy per electron).

Note that with the radiation term, the derivation of (A6) involved the use of the wave equations so that (A6) may substitute for one of them. In the reflection layer we may drop all $\bar{F}$ terms, and (A6) gives Eq. (10) by just adding $\langle E^2\rangle/8\pi n_c$ to the Gibbs free energy per electron. In the sublayer, however, we must retain the terms linear in $\bar{F}$ because now to lowest order, $n_c\times$(A6) and the total momentum equation are not independent of each other. One could then use the difference between both [for instance, Eq. (52) in Sec. IV], where the $\bar{F}$ terms are dominant, and the momentum equation without $\bar{F}$ terms; actually, to analyze the sublayer we directly used the momentum and wave equations.

We should point out that for $\bar{E}_L \equiv 0$, the right-hand side of (A6b) can be written as the divergence of some tensor so that (A6), or its difference with the momentum equation, has a conserved quantity. Since we have $\bar{E}_L \neq 0$ in the sublayer, however, this quantity will actually take different values on either side of it [Eq. (13)], the difference not vanishing with the sublayer thickness.

[1] R. E. Kiddeer, in *Proceedings of Japan–U.S. Seminar on Laser Interaction with Matter*, edited by C. Yamanaka (Tokyo International Book Co., Tokyo, 1973), p. 331.
[2] K. Lee, D. W. Forslund, J. M. Kindell, and E. L. Lindman, Phys. Fluids **20**, 51 (1977).
[3] J. P. Freidberg, R. W. Mitchell, R. L. Morse, and L. F. Rudsinski, Phys. Rev. Lett. **28**, 795 (1972).
[4] V. L. Ginzburg, *The Propagation of Electromagnetic Waves in Plasmas* (Pergamon, New York, 1970), 2nd ed.

[5] P. Koch and J. Albritton, Phys. Rev. Lett. **32**, 1420 (1974); V. B. Gil'denburg, Zh. Eksp. Teor. Fiz. **46**, 2156 (1964) [Sov. Phys.–JETP **19**, 1456 (1964).
[6] J. R. Sanmartín and J. L. Montañés, Phys. Fluids **23**, 2413 (1980).
[7] P. Mulser and C. Van Kessel, Phys. Rev. Lett. **38**, 902 (1977); J. Virmont, R. Pellat, and P. Mora, Phys. Fluids **21**, 567 (1978).
[8] G. J. Morales and Y. C. Lee, Phys. Rev. Lett. **33**, 1016 (1974); Phys. Fluids **20**, 1135 (1977).
[9] V. B. Gil'denburg and G. M. Fraiman, Zh. Eksp. Teor. Fiz. **69**, 1601 (1975) [Sov. Phys.–JETP **42**, 816 (1975)].
[10] J. C. Adam, A. Gourdin Serveniere, and G. Laval, Phys. Fluids **25**, 376 (1982).
[11] H. Takabe and P. Mulser, Phys. Fluids **25**, 2304 (1982).
[12] W. L. Kruer, Phys. Fluids **25**, 2324 (1982).
[13] F. David, P. Mora, and R. Pellat, Phys. Fluids **26**, 747 (1983).
[14] J. Albritton and P. Koch, Phys. Fluids **18**, 1136 (1975); T. Speziale and P. J. Catto, Phys. Fluids **21**, 681 (1979); W. L. Kruer, Phys. Fluids **22**, 1111 (1979).
[15] D. W. Forslund, J. M. Kindell, K. Lee, E.L. Lindman, and R. L. Morse, Phys. Rev. A **11**, 679 (1975).
[16] T. Speziale and J. P. Catto, Phys. Fluids **20**, 990 (1977).
[17] J. R. Sanmartín and J. L. Montañés, J. Plasma Phys. **23**, 349 (1980).
[18] L. D. Landau and E.M. Lifshitz, *Fluid Mechanics* (Pergamon, New York, 1987), 2nd ed.
[19] D. T. Atwood, D. W. Sweeny, J. M. Auerbach, and P. H. Y. Lee, Phys. Rev. Lett. **40**, 184 (1978); J. Briand, M. El Tamer, V. Adrian, A. Gomes, Y. Quemener, J. C. Kieffer, and J. P. Dinguirard, Phys. Fluids **27**, 2588 (1984); K. G. Estabrook, E.J. Valeo, and W. L. Kruer, Phys. Fluids **18**, 1151 (1975); O. Willi, R. G. Evans, and A. Raven, Phys. Fluids **23**, 2061 (1980); R. Fedosejevs, M. D. J. Burgess, G. D. Enright, and M. C. Richardson, Phys. Fluids **24**, 537 (1981).
[20] J. A. Stamper, Phys. Fluids **18**, 735 (1975).